Specific energy consumption of vacuum filtration: Experimental evaluation using a pilot-scale horizontal belt filter

Huttunen Manu, Nygren Lauri, Kinnarinen Teemu, Ekberg Bjarne, Lindh Tuomo, Ahola Jero, Karvonen Vesa, Häkkinen Antti

DOI: 10.1080/07373937.2019.1581214

Please cite the publication as follows:

Huttunen M. Nygren L., Kinnarinen T., Ekberg B., Lindh T., Ahola J., Karvonen V., Häkkinen A. (2019). Specific energy consumption of vacuum filtration: Experimental evaluation using a pilot-scale horizontal belt filter. Drying Technology. DOI: 10.1080/07373937.2019.1581214

This is an original manuscript of an article published by Taylor & Francis in Drying Technology on March 7, 2019, available online: http://www.tandfonline.com/doi/full/10.1080/07373937.2019.1581214.

Specific energy consumption of vacuum filtration: Experimental evaluation using a pilot-scale horizontal belt filter

Manu Huttunen[a]*, Lauri Nygren[a], Teemu Kinnarinen[b], Bjarne Ekberg [b], Tuomo Lindh[a], Jero Ahola[a], Vesa Karvonen[b], Antti Häkkinen[b]

[a]LUT School of Energy Systems, Lappeenranta University of Technology, 53850 Lappeenranta, Finland
[b]LUT School of Engineering Science, Lappeenranta University of Technology, 53850 Lappeenranta, Finland
*Corresponding author. E-mail address: manu.huttunen@lut.fi

Abstract

Horizontal belt vacuum filters are used for continuous solid-liquid separation in a wide variety of industrial processes. Despite the low pressure difference (usually $\Delta p < 0.8$ bar), the high air pumping requirement to maintain the pressure difference results in considerable energy consumption. In this paper, the specific energy consumption of vacuum filtration and air flow rates of a pilot-scale horizontal belt filter unit are investigated. The results show that a claw-type vacuum pump consumes only half the energy compared to a conventional liquid ring vacuum pump. A comparison between the specific energy consumption of vacuum filtration and thermal drying of the filter cake to zero moisture revealed that vacuum filtration accounted for less than half of the total energy consumption in the applied experimental conditions at $\Delta p = 0.2$–0.5 bar. The majority of the total pumping requirement of the pilot-scale filter resulted from leaks, and only 2–25 % of the air flow found its way through the cake and the filter medium. The results suggest that there is a combination of the pressure difference level and the mass of cake deposited per unit area that together with thermal drying consumes the least amount of energy per solids mass.

Keywords: Energy conservation; Specific energy consumption; Vacuum filtration; Horizontal belt vacuum filter; Cake dewatering; Thermal drying

1. Introduction

In recent years, the importance of energy consumption and energy efficiency of filtration processes has been recognized. Research on a limited number of filtration applications with respect to energy consumption has been reported, including filtration of fine calcium carbonate with an integrated filtration equipment [1], membrane filtration processes for harvesting of microalgae [2–4], and desalination of water [5–12]. However, the energy consumption of vacuum filtration in solid liquid separation processes has not been discussed in the literature, with the exception of the authors' laboratory-scale study [13] on the isentropic energy consumption of vacuum dewatering. Research trends and research focus in vacuum filtration has been studied by Karvonen et al. [14].

Vacuum belt filters are used in minerals processing, mining, and various fields of chemical industry for solid-liquid separation of slurries containing relatively coarse solids. The main benefits of vacuum belt filters include continuous operation, good opportunities for cake washing, and ease of monitoring and control of the separation process [15, 16]. The solids throughput of a vacuum belt filter depends only on the solids content and the feed rate of the slurry, whereas the final moisture content of the cake also depends on other properties of the slurry, such as particle size distribution and particle shape, and operating factors of the filtration process, such as the applied pressure difference, filtration time and dewatering time. In most industrial installations, the moisture content of the product is the quality parameter that sets limits on the production capacity and determines the energy consumption of the filter. The energy issues have become increasingly important in the industry as companies attempt to reduce their operational costs and environmental impacts.

Vacuum pumps typically consume most of the energy required by vacuum filters. The energy consumption of a vacuum pump is typically 2–15 kW/m^2 of the filter area, while other devices such as cloth drive and filtrate pumps consume only 0.2–0.4 kW/m^2 [17]. Therefore, optimization of the vacuum pump energy consumption can often lead to significant energy savings. When the filter cake is not washed, the separation process in a vacuum belt filter can be divided into two stages: filtration and dewatering. The aim of the filtration stage is to remove liquid from the slurry until a filter cake is formed. Problems in the filtration and dewatering stages may be caused for instance by the presence of fine particles, a wide particle size distribution, and an unfavorable particle shape [18, 19]. After the cake formation, air displaces liquid from the largest pores of the cake, provided that a cake-specific threshold pressure is exceeded [20, 21], and starts to flow through the cake at an increasing flow rate as a larger fraction of the total pore volume becomes empty of liquid [22]. As the air flow increases, the rate of dewatering decreases gradually until the saturation of the cake reaches an irreducible level [20, 23]. The energy consumption per mass unit of liquid removed increases sharply at this stage as a result of the slowdown of the liquid flow rate and acceleration of the air flow rate as demonstrated previously by the authors [13]. The final moisture content of the cake depends on the cake properties and the applied pressure [24–26], the former being also influenced by the latter. According to Kemp [27, 28], a primary method of reducing the energy consumption of thermal drying of materials is efficient upstream dewatering prior to the drying stage.

The main objective of this paper is to investigate the energy consumption and enable energy conservation of cake dewatering using a pilot-scale vacuum belt filter equipped with the instrumentation required for process control and data acquisition. In addition to examining the influence of the process variables on the specific energy consumption, the paper provides

information of energy consumption of two different types of vacuum pumps and shows a comparison between air dewatering and thermal drying of filter cakes. The effects of the mass of cake deposited per unit area on the moisture content of the filter cake, the energy consumption of filtration, and the air flow through the filter cake are studied. However, the influences of the particle size distribution and slurry solids content on the energy consumption fall outside the scope of this paper. A further objective of this paper is to compare the energy consumption of vacuum dewatering with the energy consumption of subsequent thermal drying.

2. Theory

2.1. Determination of filtration characteristics

The filtration equation used for calculation of the average specific cake resistance in constant pressure is based on Darcy's law, and after integration the equation becomes [29]

$$\frac{t}{V} = \frac{\alpha_{\mathrm{av}} \mu c}{2A^2 \Delta p} V + \frac{\mu R_m}{A \Delta p}, \tag{1}$$

where t is time elapsed since the start of the constant pressure period, V is the volume of filtrate, α_{av} is the average specific resistance of the cake, μ is the dynamic viscosity of filtrate, c is the mass of dry cake divided by the volume of filtrate, A is the effective filtration area, Δp is the pressure difference, and R_m is the resistance of the filter medium.

When only the resistance of the filter cake is considered, the equation can be simplified to the form

$$\alpha_{\mathrm{av}} = \frac{2aA^2 \Delta p}{\mu c}, \tag{2}$$

where a is the slope of the linear part of the experimentally obtained curve t/V vs. V.

For practical cases of compressible filtration, the variations of α can be presented by a power law type relationship [30]

$$\alpha = \alpha_0 \Delta p^n, \tag{3}$$

where α_0 is the specific resistance at unit applied pressure, which is obtained together with n by extrapolation and calculation from experimental data.

The average cake porosity can be calculated either by dividing the void volume of the cake by the total volume of the cake, or by subtracting the solids volume from the total volume using the formula [30]

$$\varepsilon_{\mathrm{av}} = 1 - \frac{m_{\mathrm{s}}}{\rho_{\mathrm{s}} A L}, \tag{4}$$

where m_{s} is the mass of solids, ρ_{s} is the density of solids, and L is the thickness of the filter cake. Equation (4) can be written for the case of a horizontal belt filter as

$$\varepsilon_{\mathrm{av}} = 1 - \frac{s q_{\mathrm{m,sl}}}{\rho_{\mathrm{s}} h_{\mathrm{B}} v_{\mathrm{B}} L}, \tag{5}$$

where s is the mass fraction of solids in the slurry, $q_{\mathrm{m,sl}}$ is the feed rate of the slurry in kg/s, ρ_{s} is the density of solids, h_{B} is the filter belt width, and v_{B} is the filter belt linear velocity.

2.2. Cake dewatering

Darcy's law is based on experiments on water flow through a bed of sand placed in a vertical iron pipe. The equation describing the observed relationship can be written as

$$u = \frac{-k}{\mu} \frac{dp}{dz}, \tag{6}$$

where dp is the dynamic pressure difference across the thickness dz of a porous medium of the permeability k, and u is the superficial velocity of liquid with a viscosity μ flowing through the bed [30].

In vacuum filtration, two immiscible fluids, gas and liquid, flowing through the filter medium form their unique pathways, which alter as the fluid saturation changes during filtration. As the liquid saturation is reduced to the minimum, the liquid pathways become discontinuous, the flow of the wetting fluid ceases, and the cake is at its irreducible wetting fluid saturation [30].

When Darcy's law is applied to each flowing phase, filtrate (l), and gas (g):

$$u_{\mathrm{l}} = \frac{-k_{\mathrm{l}}}{\mu_{\mathrm{l}}}\frac{dp_{\mathrm{l}}}{dz}, \tag{7}$$

and

$$u_{\mathrm{g}} = \frac{-k_{\mathrm{g}}}{\mu_{\mathrm{g}}}\frac{dp_{\mathrm{g}}}{dz}, \tag{8}$$

where dp_{l} and dp_{g} are the dynamic pressure differences across the thickness dz of a porous medium of permeabilities k_{l} and k_{g}, and u_{l} and u_{g} are the superficial velocities of the fluid with viscosities μ_{l} and μ_{g} flowing through the bed. Each phase has its own associated pressure, viscosity, and permeability. The difference between the two pressures is the capillary pressure, which is relative to the radius of the curvature of the interface between the phases, and it is dependent on the saturation of each phase. The terms k_{l} and k_{g} are effective permeabilities of the liquid and gas phases, respectively, and they are related to the permeability of the saturated medium through

$$k_{\mathrm{rl}} = k_{\mathrm{l}}/k \text{ and } k_{\mathrm{rg}} = k_{\mathrm{g}}/k, \tag{9}$$

where k_{rl} *and* k_{rg} are the cake relative permeabilities to the liquid and gas phases, respectively [30].

Darcy's equations for the flow of the two phases through the cake combined with the material balances for each phase give

$$\frac{\partial(\varepsilon S)}{\partial t} = -\frac{\partial u_\mathrm{l}}{\partial z} \tag{10}$$

and

$$\frac{\partial\left(\varepsilon\rho_\mathrm{g}(1-S)\right)}{\partial t} = -\frac{\partial\left(\rho_\mathrm{g}u_\mathrm{g}\right)}{\partial z}. \tag{11}$$

Using Eqs. (1) – (5) and solving the partial differential equations with boundary conditions for a particular operating point of the vacuum filter, one can calculate the final saturation of the filter cake and the gas and liquid flow through the cake. To facilitate these calculations, the equations have been solved, presented graphically, and curve fitted to a dimensionless form by [30]. Using these fittings, the reduced saturation S_R and the gas flow rate u_g through the cake can be estimated with the following simplified calculations.

Dimensionless terms used to calculate dewatering dynamics are written in terms of the average permeability k_av of the filter cake

$$k_\mathrm{av} = \frac{1}{\alpha_\mathrm{av}\rho_\mathrm{s}(1-\varepsilon_\mathrm{av})}, \tag{12}$$

where α_av is the average specific cake resistance, ρ_s is the density of solids, and ε_av is the average cake porosity.

Dimensionless deliquoring time θ is defined by

$$\theta = \frac{k_\mathrm{av}p_\mathrm{b}}{\mu_\mathrm{l}\varepsilon_\mathrm{av}(1-S_\infty)L^2}t_\mathrm{d}, \tag{13}$$

where p_b is the threshold pressure at which the flow of the liquid begins, S_∞ is the irreducible saturation at which the flow of the liquid ceases, L is the height of the cake, and t_d is the deliquoring time in seconds.

The threshold pressure p_b can be calculated by the equation

$$p_b = \frac{4.6(1-\varepsilon_{av})\sigma}{\varepsilon_{av} x}, \tag{14}$$

where σ is the cake liquid surface tension and x is the particle mean diameter.

The dimensionless gas flux u_g^* is calculated by

$$u_g^* = \frac{u_g \mu_g L}{k_{av} p_b}. \tag{15}$$

the dimensionless pressure p^* is calculated by dividing the pressure p by the threshold pressure:

$$p^* = \frac{p}{p_b}. \tag{16}$$

A value for the filter cake saturation is obtained by first determining a value for the reduced saturation S_R from Fig. 1 and applying it to the equation

$$S = S_\infty + S_R(1-S_\infty). \tag{17}$$

To evaluate a design gas flow rate u_g for vacuum pump or blower specification, the following calculations can be carried out. The dimensionless pressure difference across the cake is

$$p_g^* = p_{gei}^* - p_{geo}^* = \frac{p_B}{p_b} - \frac{p_B - \Delta p_d}{p_b} = \frac{\Delta p_d}{p_b}, \tag{18}$$

where the subscript g denotes pressure in the gas phase, i indicates the entry surface of the cake and o the exit surface of the cake in terms of gas flow direction, and e stands for the actual filter installation. The averaged dimensionless gas flow rate $\bar{u}_g^*$ is obtained from Fig. 2, and the superficial gas velocity u_g is calculated by using Eqs. (19) and (20)

This is an original manuscript of an article published by Taylor & Francis in Drying Technology on March 7, 2019,
available online: http://www.tandfonline.com/doi/full/10.1080/07373937.2019.1581214.

$$\bar{u}^*_{\mathrm{ge}} = \bar{u}^*_{\mathrm{g}} \frac{p^*_{\mathrm{go}}}{p^*_{\mathrm{geo}}} \left[\frac{\left(p^*_{\mathrm{geo}}\right)^2 - \left(p^*_{\mathrm{gei}}\right)^2}{\left(p^*_{\mathrm{go}}\right)^2 - \left(p^*_{\mathrm{gi}}\right)^2} \right], \tag{19}$$

$$u_{\mathrm{g}} = \bar{u}^*_{\mathrm{ge}} \frac{k_{\mathrm{av}} p_{\mathrm{b}}}{\mu_{\mathrm{g}} L}, \tag{20}$$

where $p^*_{\mathrm{gi}} = 100$, $p^*_{\mathrm{go}} = 100 - p^*_{\mathrm{g}}$ and μ_{g} is the gas viscosity.

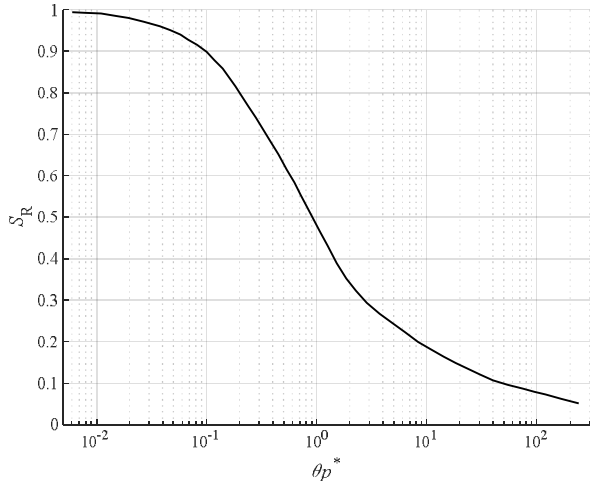

Fig. 1. Reduced saturation S_R of a filter cake as a function of the product of the dimensionless deliquoring time θ and the dimensionless pressure p^* according to [30].

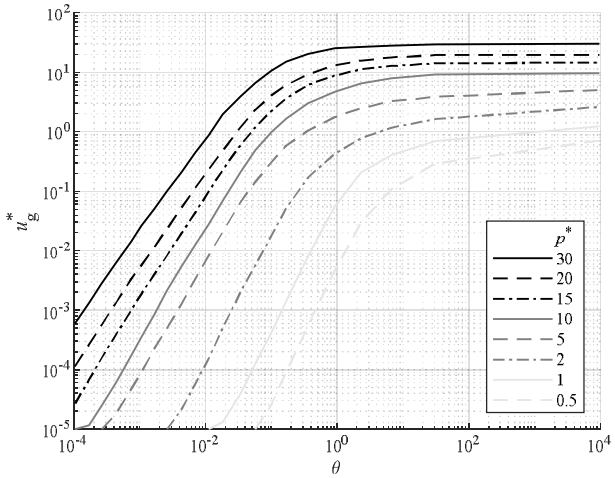

Fig. 2. Averaged dimensionless gas flow rate through the filter cake $\bar{u}^*_{\mathrm{g}}$ as a function of the dimensionless deliquoring time θ and the pressure p^* according to [30].

2.3. Power demand in vacuum filtration

In vacuum filtration, the desired pressure difference across the filter cake is generated by a vacuum pump. The ideal isentropic power demand P_S for a given inlet volumetric flow rate $q_{V,in}$ generated by the vacuum pump can be calculated by the equation

$$P_S = \frac{k}{k-1} q_{V,in} p_{in} \left[\left(\frac{p_{out}}{p_{in}} \right)^{\frac{k-1}{k}} - 1 \right], \tag{21}$$

where p_{in} is the pressure at the inlet of the vacuum pump, p_{out} is the outlet pressure of the vacuum pump, and k is the isentropic exponent. If the vacuum pump is cooled, the isothermal power demand P_T can be used to describe the ideal process, and it can be calculated using equation

$$P_T = q_{V,in} p_{in} \ln \left(\frac{p_{out}}{p_{in}} \right). \tag{22}$$

Depending on whether the isothermal or isentropic compression is assumed, the required vacuum pump shaft power can be determined by the equation

$$P_{shaft} = \frac{P_T}{\eta_T} \quad \text{or} \quad P_{shaft} = \frac{P_S}{\eta_S}. \tag{23}$$

2.4. Power demand in thermal drying

If the moisture content of the filter cake after vacuum filtration is not low enough, additional drying of the product is required. In thermal drying, the moisture is removed from the cake by evaporation. The ideal power required for evaporation can be described by the equation [28]

$$P_v = q_{m,v} \Delta H_v = q_{m,s} \left(\frac{1}{s_{in}} - \frac{1}{s_{out}} \right) \Delta H_v, \tag{24}$$

where q_m is the mass flow, ΔH_v is the latent heat of evaporation, and s is the weight-based solids content of the cake. The subscript v denotes vapor and s solids. For ideal energy consumption, it is assumed that all the supplied energy goes to the evaporation of water removed from the cake.

This includes the energy required for heating up the water from 20 to 100 °C and for evaporation (ΔH_v = 2400 kJ/kg). The energy consumed in heating of solids is neglected.

The most commonly encountered dryer in the mineral processing industry is the rotary dryer, the thermal efficiencies of which typically range from 35 to 70 % [31]. In addition to rotary dryers, other convection type dryers suitable for filter cake drying are for instance flash, fluid bed, and tray dryers [31]. According to [28], convective dryers tend to have a low thermal efficiency (often below 50 %).

3. Materials and methods

3.1. Slurry

The slurry with a total solids content of 25 wt.% was prepared from Nordkalk Parfill H80 dry solids and tap water. The solids consisted mainly of ground calcium carbonate (89 %) and small amounts of other components containing for instance Si, Al, Mg, and Na. The volumetric particle size distribution of the solids, measured by using a Malvern Mastersizer 3000 laser diffraction analyzer and shown as the average of several trials, is presented in Fig. 3. Mixing tanks equipped with propeller type impellers and baffles were used to keep the slurry mixed during the experiments.

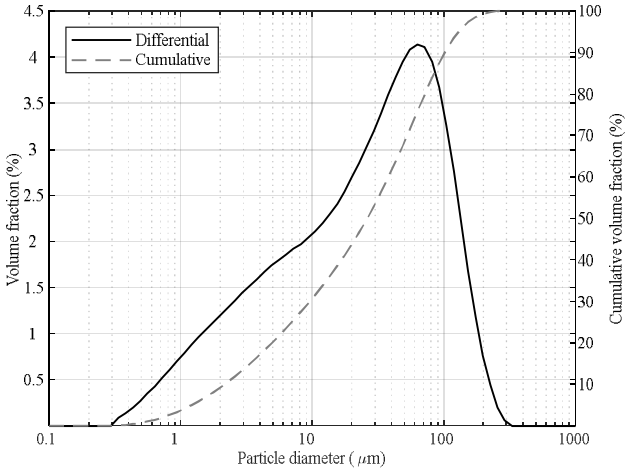

Fig. 3. Particle size distribution of Nordkalk Parfill H80.

3.2. Horizontal belt vacuum filter and related instrumentation

The horizontal belt vacuum filter used in this study and its device setup and instrumentation are illustrated in Fig. 4. The main operational parts of the machine are the slurry infeed, filter belt, vacuum generation, and filtrate handling. The physical layout of the devices is divided into three levels to enable sufficient vertical moving space for the filtrate level inside the barometric leg. The filtrate level moves inside the barometric leg according to the pressure difference applied to the filter. Manipulation of the operating point of the filter is implemented with the help of frequency-converter-operated pumps and a belt motor. The slurry infeed is controlled by two hose pumps. The first one circulates the slurry to avoid the settling of solids in the pumping line. The second pump controls the infeed flow to the filter belt, the feed flow rate being linearly proportional to the rotation speed of the pump. A vacuum is generated either with a liquid ring vacuum pump or with a claw vacuum pump. The filter has a reciprocating tray. The applied pressure difference joins the tray with the filter cloth, and thus, the tray moves with the filter belt for its operating distance of 10 cm. After this distance, the vacuum is cut off from the tray, the tray is returned to the starting

point of the movement, and the vacuum is reapplied. The filter effective length is 2.1 m and the width is 0.1 m. With the liquid ring vacuum pump, the filter is able to reach vacuum levels up to 0.4 bar and up to 0.6 bar with the claw vacuum pump.

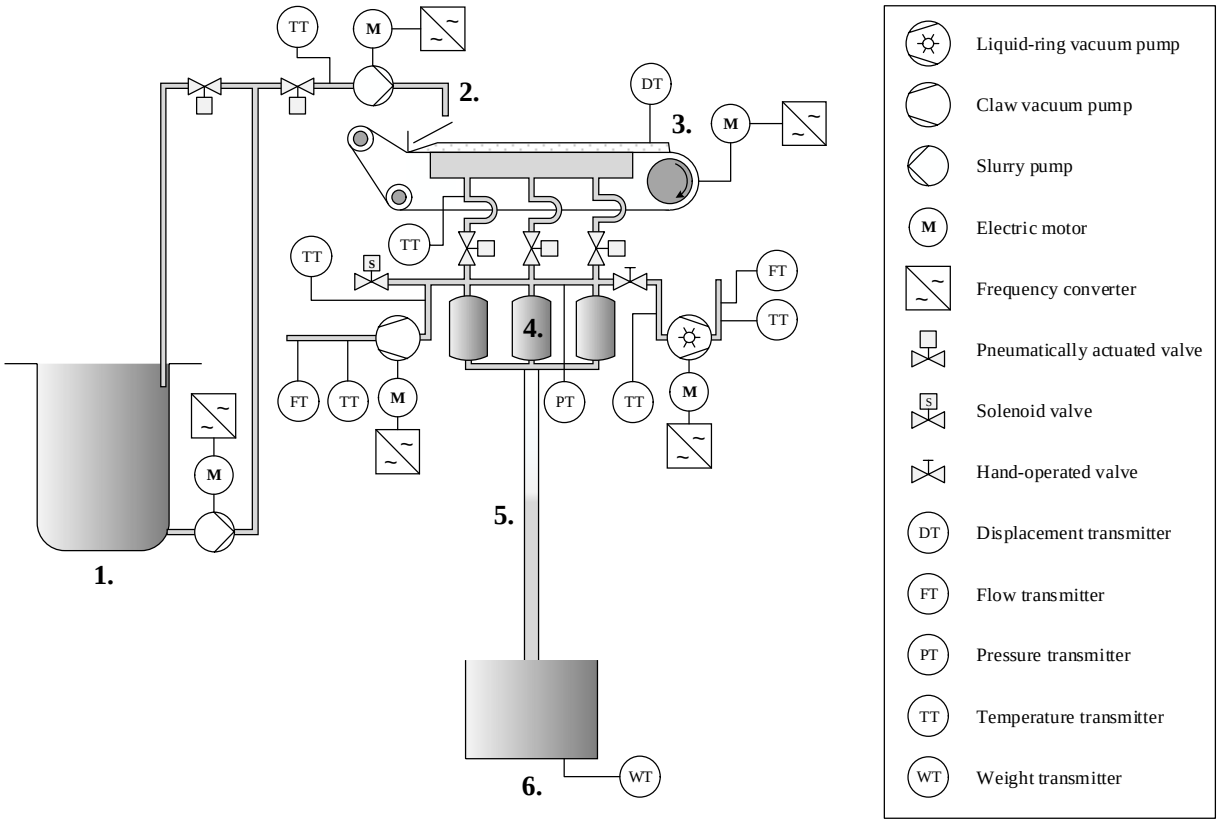

Fig. 4. Horizontal belt vacuum filter device setup and instrumentation: 1) slurry tank, 2) slurry infeed, 3) cake discharge, 4) filtrate intermediate tanks, 5) barometric leg, and 6) filtrate collection tank.

Frequency converter operation of the filter motors enables monitoring of energy consumption and calculation of the belt speed and the slurry infeed rate. Ideal energy consumption required to generate a pressure drop can be calculated on the basis of the vacuum pump flow rate and vacuum chamber pressure measurements. Vacuum pump flow rates were measured using flow velocity sensors based on the measuring principle of a thermal anemometer. The temperature measurements of the slurry infeed, the filtrate, and the vacuum pump inlet and outlet flow were collected. Filtrate

production was measured using a digital scale for the filtrate collection tank. The cake thickness at the end of the dewatering phase was measured using a laser displacement sensor.

The separation process in the filter is continuous, including the slurry distribution on the belt, filtration until the cake is formed, and dewatering (i.e. drying) until the cake is discharged at the end of the belt. The discharged cake is collected in vessels located below the filter. After the cake discharge, the filter belt is spray washed with a large amount of water until no remaining solid particles can be detected on the belt. Thus, the effect of the filter belt wash on the product quality and energy consumption is outside the scope of this study. There is also an option for cake washing and operation in an inert gas atmosphere, but those options are omitted in this study. The devices used for pilot-scale filter instrumentation are presented in Table 1.

3.3. Filtration experiments

The aim of the experimental work was to investigate the effect of the main process variables on the properties of the filter cake, as well as the air and energy consumption of dewatering, and to compare the laboratory results with those obtained by using the pilot-scale filter.

Experiments with a Büchner apparatus were conducted to determine the specific cake resistance and porosity. Pilot-scale experiments were carried out to study cake dewatering with a horizontal belt vacuum filter. A set of twelve experiments were carried out to study the effect of pressure difference and the mass of cake deposited per unit area w on the weight-based moisture content of the filtered cake and on the energy consumption of vacuum filtration. The mass of cake deposited per unit area was controlled by adjusting the slurry infeed rate and the belt speed. The experimental conditions are presented in Table 2.

4. Results

4.1. Filtration properties of the slurry

Results from the Büchner apparatus experiments are presented in Table 3. The solid content of the slurry, *s*, was constant 25 wt.% in all experiments. Shrinking of the filter cake was observed in experiments 4–9 at the beginning of the dewatering stage. The shrinking of the filter cake causes the average porosity of the cake to change during the dewatering stage. For this reason, a value of the average porosity and the cake thickness at the time of transition from the separation stage to the dewatering stage, $\varepsilon_{av,\,tr,\,calc}$, was also calculated using the volume of solids and liquid at this instance with the assumption that the cake was completely saturated. This value could be considered the initial value used for calculating the average porosity in the dewatering stage. The average specific cake resistance α_{av} was the higher, the larger was the filtration pressure difference, and thus, it can be concluded that the filter cakes were slightly compressible. The values of α_{av} were typical for vacuum filtration of calcium carbonate [32]. The capillary tests gave an average value for the irreducible saturation S_∞ of 0.61.

Results from the experiments using a pilot-scale horizontal belt filter with a liquid ring vacuum pump are presented in Table 4. The manipulated filtration variables are the pressure difference Δp and the mass of cake deposited per unit area *w*, which was adjusted with the filter belt speed v_{belt} and the slurry infeed rate. The presented properties of the filter cakes are the filtration time t_f and the distance z_f, the dewatering time t_d and the distance z_d, the cake thickness *L*, the average porosity ε_{av}, the throughput of the cake solids M_s, and the moisture content *M*. The average porosity is calculated by using the cake thickness measurement at the end of the dewatering period.

The results show that a lower moisture content and average porosity of the filter cake are achieved by increasing the pressure difference. Furthermore, the moisture content and the average porosity vary depending on the mass of cake deposited per unit area *w*, the dewatering time, and the distance. The lowest moisture content and average porosity of the filter cake for a given pressure difference level are achieved when the dewatering time is longest. When comparing Tests 6 and 8, and 9 and 12 within the same pressure difference level for which the dewatering time is close to each other or exactly the same, it is observed that a lower moisture content is achieved with a thicker cake. Comparing the experiments within the same pressure difference levels of 0.3 and 0.4 bar with the *w* of 4.2 to 5.4 and 12.2 kg/m^2, a lower moisture content is achieved with the thicker filter cake while the shorter dewatering time and distance would indicate the contrary. This would suggest that there is an optimum value for the mass of cake deposited per unit area when seeking for the best dewatering performance. A similar observation was made with a different material in the previous study of the authors [13]. It can be speculated that the reason for a poor dewatering performance of the thinnest cakes may result from the uneven air flow, which, in turn, could be caused by the lack of a sufficient capillary structure in such cakes. Additionally, one factor omitted in this study is the effect of the filter medium: it might be possible that thin cakes are not effectively dewatered because the whole height profile of the cake is simply too close to the cake/medium interface, where the cake properties do not facilitate effective dewatering. In this study, the series *w* of 9.5 kg/m^2, which also has the longest dewatering times, gives the best results in terms of moisture content.

Results from the experiments using a pilot-scale horizontal belt filter with a claw vacuum pump are presented in Table 5. Similar results as with the liquid ring vacuum pump were achieved with the claw vacuum pump; a lower moisture content is achieved with a thicker cake. For this

experiment series with Δp between 0.2 and 0.4 bar, the w of 10.3 kg/m^2 having the longest dewatering times gives the best results in terms of moisture content after dewatering. The lowest average porosity values for the claw vacuum pump experiments remained higher compared with the liquid ring pump experiments. The main reason for this is probably the slightly higher solids content of the slurry in the experiments with the claw pump. Increasing the solids content of the slurry typically results in a more rapid cake formation and a higher porosity.

4.2. Air flow rates

Volumetric air flow rates calculated from the flow velocity measurements of the pilot-scale experiments are presented in Table 6. To determine the leak flow of the horizontal belt filter vacuum system for the pressure difference region used in the experiments, a series of test runs were conducted. The infeed of the slurry and the speed of the filter belt were adjusted so that the filter cake was 100 % saturated over the whole area affected by the pressure difference. In this operating point, the fluid flow through the cake was assumed to be so low that it can be ignored and the air flow through the vacuum pump can be considered to originate from the vacuum system leaks. Linear correlation for the vacuum system leak flow with respect to the pressure difference across the filter cake is presented in Fig. 5. The behavior of vacuum system leaks in a standard volumetric air flow through the vacuum pump is linear as a function of pressure difference across the filter cake with a root-mean-squared error of 0.414, R-squared 0.998, and a p-value of $3.1 \cdot 10^{-5}$. Test 4 in both experiment series has a fully saturated filter cake along the whole distance of the filter belt. The air flow rate through the cake is zero in these tests, and the total air flow value serves as a reference point in determining the leak flow with the linear regression model for the other tests in the series.

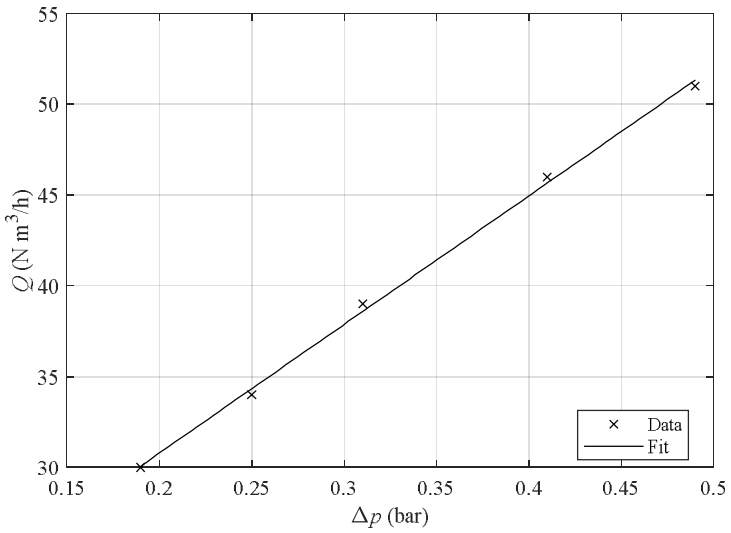

Fig. 5 Linear correlation for the leak air flow of the vacuum system of the pilot-scale belt filter with respect to the pressure difference across the filter cake.

The corresponding dimensionless dewatering time, pressure, and air flow rate for the experiments calculated using Eqs. (2)–(5), (12)–(16), and (18)–(20) and the results from Table 3–Table 6 are presented in Fig. 6. This representation of the results is analogous to Fig. 2. The average porosity value used for the calculations is an average value of $\varepsilon_{\mathrm{av,\,tr,\,calc}}$ of the Büchner experiments 1–9 (excluding the outlier Test 7) and the final average porosity, $\varepsilon_{\mathrm{av}}$, of each pilot filter test. By comparing the results presented in Fig. 2 with the same mass of cake deposited per unit area w in Fig. 6, it can be seen that the material used in the pilot-scale experiments shows a similar trend of the averaged dimensionless air flow rate as the theoretical curve. However, when the mass of cake deposited per unit area is increased from 4.6 to 10.3 kg/m^2, the averaged dimensionless air flow rate increases even if the dimensionless pressure decreases at the same time. Fig. 6 together with Table 6 also shows that increasing the mass of cake deposited per unit area within the same pressure difference level Δp increases the average air flux through the cake $u_{\mathrm{a,\,cake}}$.

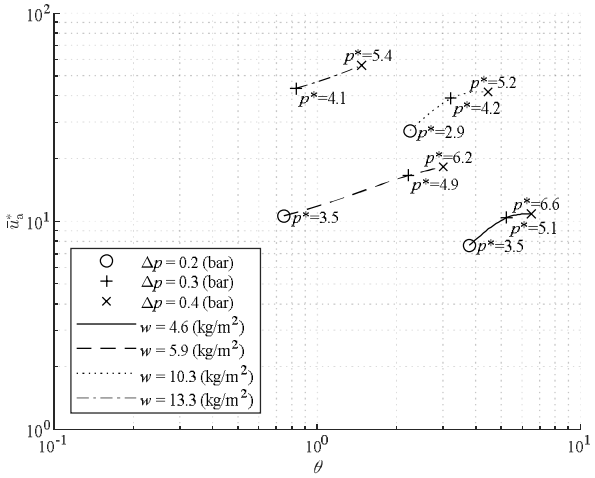

Fig. 6 Dimensionless air flow rates $\bar{u}_a^*$ with respect to the dimensionless deliquoring time θ for the horizontal belt filter and claw vacuum pump experiments calculated using Eqs. (2)–(5), (12)–(16), and (18)–(20).

4.3. Variations in the pressure difference

The cut-off and cut-in of suction to the vacuum box for the duration of the tray return movement induces transients to the pressure difference between the vacuum box and the ambient atmospheric pressure affecting through the filter cake as well as to the standard volumetric air flow rates. These transients, again, cause oscillation to the water level inside the barometric leg. The effect of these phenomena on the pressure difference can be seen in Fig. 7 (a) and on the standard volumetric air flow rates in Fig. 7 (b). To limit the water level oscillations inside the barometric leg, a diameter of 7 cm is selected for the barometric leg and an adjustable and controllable bypass valve is used to let air flow to the vacuum pump during the vacuum box suction cut-off. As can be seen in Fig. 7 (b), the slowdown in the air flow rate induced by the resistance of the bypass valve is more significant at higher pressure differences and flow rates. Fig. 7 (a) illustrates the corresponding increase in the pressure difference.

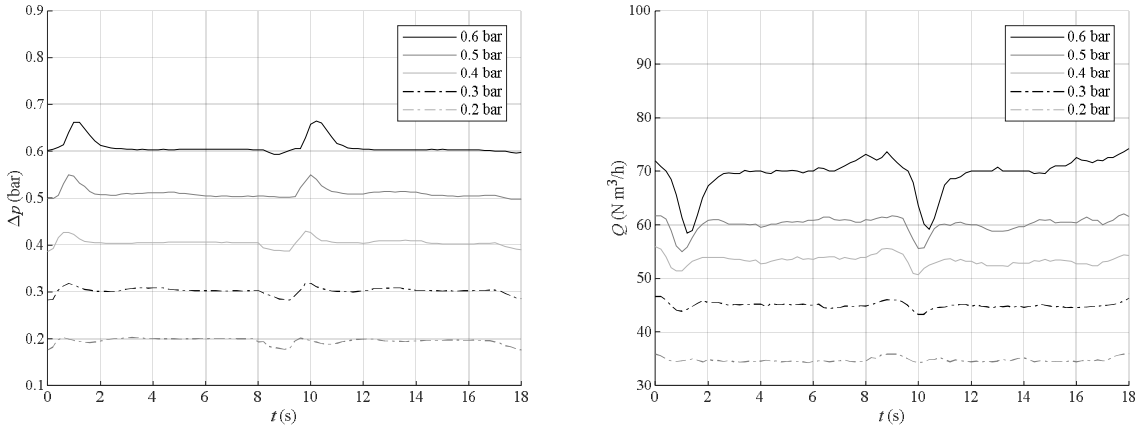

a) b)

Fig. 7 Example of transients in the pressure difference affecting the filter cake a) and in the standard volumetric air flow rate through the vacuum pump b). A sequence from claw pump experiments 1, 5, 9, 13, and 15.

4.4. Product quality and energy consumption

Fig. 8–10 present the specific energy consumption, $E_s = E/m_s$, for the pilot-scale horizontal belt filter experiments. Fig. 8 depicts the total ideal specific energy consumption for the claw pump experiments calculated using the air flow measurements and the isentropic power demand (Eq. (21)) and thermal drying to the zero moisture content with a thermal efficiency η_{th} = 100 % (Eq. (24)). The minimum total ideal energy consumption is achieved with Test 3 and values close to this one with Tests 6, 7, and 8 (see Table 6). Keeping the pressure difference and the belt speed fixed and increasing the mass of cake deposited per unit area decreases the ideal specific energy consumption of vacuum filtration. Moreover, with the exception of Test 4, where the filter cake does not have the chance to be dewatered with the vacuum filter, the total ideal energy consumption is decreased.

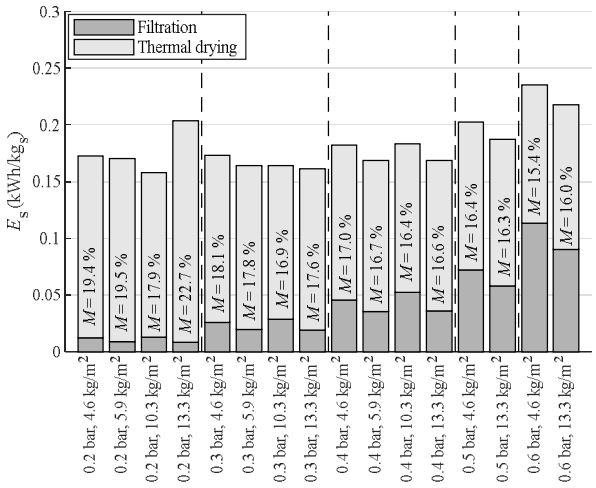

Fig. 8 Ideal specific energy consumption for achieving zero moisture content (M = 0 %) distinguishing between vacuum filtration and thermal drying (thermal efficiency η_{th}=100 %). The moisture content after vacuum filtration is shown for each experiment.

Fig. 9 presents the specific energy consumption of solid-liquid separation using a horizontal belt vacuum filter with a liquid ring vacuum pump in the first stage and thermal drying in the second stage to obtain the desired final zero moisture content. The corresponding results for the dry claw vacuum pump experiments are shown in Fig. 10. The energy consumption for filtration was calculated on the basis of power consumption data provided by the variable speed drive. The assumed thermal efficiency η_{th} = 50 % used for the thermal drying calculations is based on the heat efficiency of a spin-flash dryer reported by Kudra et al. [33]. The illustrations in Fig. 9 indicate that the minimum specific energy consumption to attain a zero moisture content with the liquid ring pump is reached in Test 3 with a 0.2 bar pressure difference and 9.5 kg of cake deposited per unit area. The specific energy consumption close to the minimum is also achieved with Tests 2, 6, and 8. As with the ideal case presented in Fig. 8, keeping the pressure difference and the belt speed fixed and increasing the mass of cake deposited per unit area decreases the specific energy consumption of vacuum filtration, and with the exception of Test 4, also the total energy consumption is decreased.

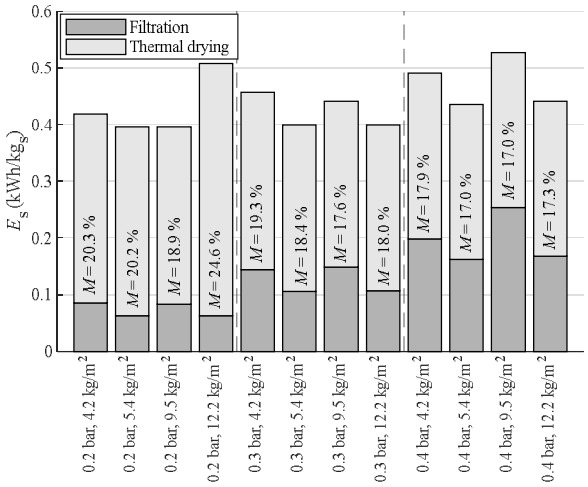

Fig. 9 Specific energy consumption for achieving zero moisture content (M = 0 %) for liquid ring vacuum pump experiments. Distinguishing between vacuum filtration and thermal drying (thermal efficiency η_{th}=50 %). The moisture content after vacuum filtration is shown for each experiment.

Fig. 10 indicates that the minimum specific energy consumption to attain a zero moisture content with the claw pump is achieved in Test 3 using a 0.2 bar pressure difference and 10.3 kg of cake deposited per unit area. The specific energy consumption close to the minimum is also reached in Tests 6 and 8. As can be observed in Fig. 10, it is not energy efficient to dewater the filter cake to the lowest achievable moisture content by using a high pressure difference. The highest specific energy consumption of the overall dewatering and drying process is caused by the unsuitable combination of a low solids loading and a high pressure difference. On the other hand, thermal drying of excessively wet filter cakes cannot be recommended when targeting at a low total energy consumption. The specific energy consumption of the claw vacuum pump is analogous to that of the liquid ring pump in the sense that keeping the pressure difference and the belt speed fixed and increasing the mass of cake deposited per unit area decreases the specific energy consumption of vacuum filtration. Additionally, with the exception of Test 4, the total energy consumption is decreased. Mainly because of the higher efficiency of the claw vacuum pump, the specific energy

consumption of vacuum filtration is roughly half of that of the liquid ring pump operated at the same pressure difference.

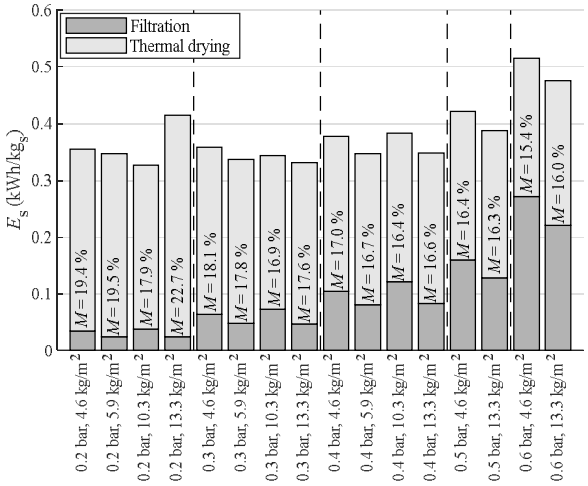

Fig. 10 Specific energy consumption for achieving zero moisture content (M = 0 %) for claw vacuum pump experiments. Distinguishing between vacuum filtration and thermal drying (thermal efficiency η_{th}=50 %). The moisture content after vacuum filtration is shown for each experiment.

A comparison of the measured specific energy consumptions obtained with the two types of pumps and the ideal isentropic specific energy consumption of cake dewatering (excl. thermal drying) is presented in Fig. 11. As mentioned above, cake dewatering with the liquid ring vacuum pump (LRVP) requires considerably more energy than dewatering with the claw pump. In addition to the comparison between the two different pump types, two alternative vacuum level control strategies using the liquid ring pump are compared. The bypass control strategy is implemented by running the pump at a full speed and inducing leak air flow into the vacuum system through a bypass valve, whereas the use of a variable speed drive (VSD) enables vacuum level control by manipulating the rotation speed of the vacuum pump directly. It is clearly illustrated in Fig. 9 that the use of a VSD reduces the specific energy consumption in cases where the pressure difference is small, and thus, below the maximum pressure difference obtainable by the pump. In this study,

the maximum pressure difference obtainable by the LRVP was approximately 0.4 bar, which explains the negligible energy savings achieved by the use of a VSD when operating at Δp = 0.4 bar.

The ideal specific energy consumption in Fig. 11 was calculated using the isentropic power demand (Eq. (21)) and the air flow measurements from the claw vacuum pump experiments. Because of the efficiencies of the vacuum pumps, the ideal specific energy consumption is less than half of the actual energy consumption of the claw vacuum pump and less than one-quarter of the actual energy consumption of the liquid ring vacuum pump.

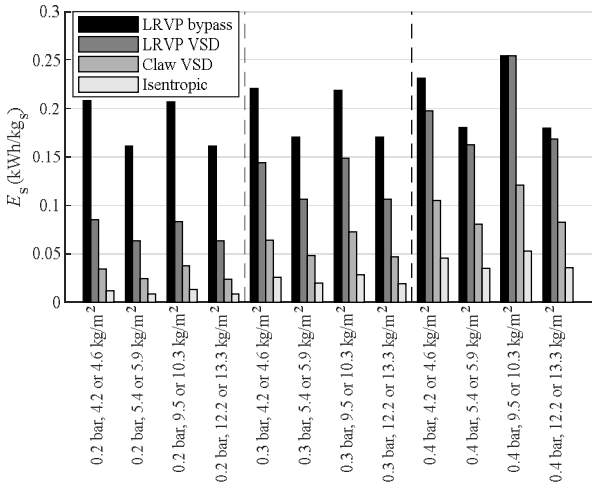

Fig. 11 Comparison of the specific energy consumption of filter cake dewatering with a horizontal belt vacuum filter. Dewatering by a liquid ring vacuum pump (LRVP) with a bypass valve and a variable speed drive (VSD) for pressure difference control. Dewatering by a claw vacuum pump with a variable speed drive (VSD) for pressure difference control. Ideal specific energy consumption of filter cake dewatering calculated using the isentropic power demand and the air flow measurements from the claw vacuum pump experiments.

5. Discussion

To reach a moisture level of zero percent with the combination of vacuum filtration and thermal drying, the specific energy consumption of vacuum filtration varies between 7 and 53 percent of the total specific energy consumption depending on the applied pressure difference. The lowest total specific energy consumptions are achieved with the pressure difference levels of 0.2 and 0.3 bar. The standard volumetric leak flow of the vacuum system of the pilot-scale vacuum filter used for the experiments increases linearly as a function of applied pressure difference. The increased air leak flow and the increased air flow through the filter cake have a nonlinear effect on the power demand and energy consumption of vacuum filtration as can be seen in Eqs. (21) and (22). The efficiency of vacuum pumps also behaves nonlinearly as a function of compression ratio [34, 35]. According to the experiments carried out with the pilot-scale horizontal belt vacuum filter, the specific energy consumption of vacuum filtration has a tendency to increase exponentially as the pressure difference is increased. A lower moisture content after vacuum filtration is achieved with a higher pressure difference, but the increased specific energy consumption of vacuum filtration adds to the total specific energy consumption with thermal drying to the extent that it is above optimal when the applied pressure difference is 0.4 bar or higher.

The claw vacuum pump used for the experiments has a significantly higher efficiency compared with the liquid ring vacuum pump. Typically, liquid ring vacuum pumps have been used in filtration because of their ability to handle condensable vapors and availability for large capacities. Liquid ring pumps are available to capacities of over 37 000 m^3/h, while dry pumps are available only up to 2400 m^3/h [35]. The required capacities in vacuum filtration are often very high as a

result of air flow from the leaks and through the cake; for instance in [36], for a 94 m^2 filter area, a vacuum pump with a suction capacity of 7000 m^3/h was used with a 0.45 bar pressure difference.

Controlling the vacuum level with a bypass valve should be avoided at all cost because of the high amount of energy wasted compared with controlling the vacuum level with a variable-speed-drive-operated vacuum pump. By adjusting the slurry infeed, the filter belt speed, and the vacuum level with variable speed drives, the moisture content of the filter cake could be controlled and the energy consumption of vacuum filtration could be optimized.

In process configurations where it is feasible to convey the filtrate flow several meters downwards inside a barometric leg, it might be possible to eliminate the energy consumption of filtrate pumping. Other devices in a horizontal belt vacuum filter besides the vacuum pump, such as cloth drive and filtrate pumps, typically consume 0.2–0.4 kW/m^2 of power [17]. This would make the energy saving potential of the barometric leg less than 0.2–0.4 kW/m^2. The use of the barometric leg could save energy by eliminating the need for a filtrate pump, but it also induces minor oscillation to the vacuum pressure, the air flow through the vacuum pump, and the filtrate level inside the barometric leg.

Using the method for identification of the leak flow of the vacuum system described in this article enables condition monitoring of the filter vacuum system and estimation of the flow through the filter cake. By this estimation, one could also calculate the efficiency of a vacuum filter for example in terms of the ratio of the leak flow and the flow through the filter cake.

6. Conclusions

According to the experiments carried out in this study, the main factors in minimizing the specific energy consumption of vacuum filtration are the usage of a variable-speed-controlled vacuum pump for controlling the pressure difference, the application of a moderate pressure difference of 0.2 to 0.3 bar, and the usage of an efficient vacuum pump. Claw-type vacuum pumps are more favorable than liquid ring pumps from the efficiency and energy consumption points of view.

The isentropic specific energy consumption calculated from the air flow data was significantly lower than the actual energy consumption obtained from the frequency converter. The vacuum system leak flow plays a considerable role in the total specific energy consumption of vacuum belt filters. However, the leak flow from the edges of the filter cloth is not as great in large plant-scale filters, where the ratio between the edge length and the filtration area is smaller than in the pilot-scale filter used in this study.

The results of this study support the general assumption that thermal drying consumes the majority of the total energy consumption when dry solids are produced by a combination of mechanical solid-liquid separation and thermal drying. Furthermore, the results suggest that there is a combination of the pressure difference level and the mass of cake deposited per unit area that minimize the total energy consumption per solids mass of the filtration and thermal drying phases. For the experiments carried out in the study, taking into consideration also the throughput of cake solids, the most advantageous combination was to generate a 0.3 bar pressure difference with the claw vacuum pump and feed the slurry at the rate of 13.3 kg of cake deposited per unit area, which corresponded to a cake height of approximately 7.7 mm.

Acknowledgments

The authors would like to thank Hanna Niemelä for providing language help and The Finnish Funding Agency for Technology and Innovation (Tekes) for providing funding for the study.

References

[1] Zhu, Y.-F.; Qian, J.-Y.; Zhang, Q.-K.; Kuang, J.-Y.; Gao, X.-F.; Jin, Z.-J. Experimental Analysis on Filter Press and Energy Consumption Performance of Diaphragm Press Drying Device in Chemical Post-Processing Integrated Equipment. *Case Stud. Therm. Eng.* **2016**, *7*, 92–102. DOI: 10.1016/J.CSITE.2016.03.004.

[2] Eliseus, A.; Putra, Z. A.; Bilad, M. R.; Nordin, N. A. H. M.; Wirzal, M. D. H.; Jaafar, J.; Khan, A. L.; Aqsha. Energy Minimization of a Tilted Panel Filtration System for Microalgae Filtration: Performance Modeling and Optimization. *Algal Res.* **2018**, *34*, 104–115. DOI: 10.1016/J.ALGAL.2018.07.008.

[3] Danquah, M. K.; Ang, L.; Uduman, N.; Moheimani, N.; Forde, G. M. Dewatering of Microalgal Culture for Biodiesel Production: Exploring Polymer Flocculation and Tangential Flow Filtration. *J. Chem. Technol. Biotechnol.* **2009**, *84* (7), 1078–1083. DOI: 10.1002/JCTB.2137.

[4] Bilad, M. R.; Discart, V.; Vandamme, D.; Foubert, I.; Muylaert, K.; Vankelecom, I. F. J. Harvesting Microalgal Biomass Using a Magnetically Induced Membrane Vibration (MMV) System: Filtration Performance and Energy Consumption. *Bioresour. Technol.* **2013**, *138*, 329–338. DOI: 10.1016/J.BIORTECH.2013.03.175.

[5] Karabelas, A. J.; Koutsou, C. P.; Kostoglou, M.; Sioutopoulos, D. C. Analysis of Specific Energy Consumption in Reverse Osmosis Desalination Processes. *Desalination* **2018**, *431*, 15–21. DOI: 10.1016/J.DESAL.2017.04.006.

[6] Zarzo, D.; Prats, D. Desalination and Energy Consumption. What Can We Expect in the near Future? *Desalination* **2018**, *427*, 1–9. DOI: 10.1016/J.DESAL.2017.10.046.

[7] Mazlan, N. M.; Peshev, D.; Livingston, A. G. Energy Consumption for Desalination — A Comparison of Forward Osmosis with Reverse Osmosis, and the Potential for Perfect Membranes. *Desalination* **2016**, *377*, 138–151. DOI: 10.1016/J.DESAL.2015.08.011.

[8] Sarai Atab, M.; Smallbone, A. J.; Roskilly, A. P. An Operational and Economic Study of a Reverse Osmosis Desalination System for Potable Water and Land Irrigation. *Desalination* **2016**, *397*, 174–184. DOI: 10.1016/J.DESAL.2016.06.020.

[9] Ghaffour, N.; Missimer, T. M.; Amy, G. L. Technical Review and Evaluation of the Economics of Water Desalination: Current and Future Challenges for Better Water Supply Sustainability. *Desalination* **2013**, *309*, 197–207. DOI: 10.1016/J.DESAL.2012.10.015.

[10] Al-Karaghouli, A.; Kazmerski, L. L. Energy Consumption and Water Production Cost of Conventional and Renewable-Energy-Powered Desalination Processes. *Renew. Sustain. Energy Rev.* **2013**, *24*, 343–356. DOI: 10.1016/J.RSER.2012.12.064.

[11] Avlonitis, S. A.; Kouroumbas, K.; Vlachakis, N. Energy Consumption and Membrane Replacement Cost for Seawater RO Desalination Plants. *Desalination* **2003**, *157* (1–3),

151–158. DOI: 10.1016/S0011-9164(03)00395-3.
[12] Zhao, R.; Porada, S.; Biesheuvel, P. M.; van der Wal, A. Energy Consumption in Membrane Capacitive Deionization for Different Water Recoveries and Flow Rates, and Comparison with Reverse Osmosis. *Desalination* **2013**, *330*, 35–41. DOI: 10.1016/J.DESAL.2013.08.017.
[13] Huttunen, M.; Nygren, L.; Kinnarinen, T.; Häkkinen, A.; Lindh, T.; Ahola, J.; Karvonen, V. Specific Energy Consumption of Cake Dewatering with Vacuum Filters. *Miner. Eng.* **2017**, *100*, 144–154. DOI: 10.1016/J.MINENG.2016.10.025.
[14] Karvonen, V.; Huttunen, M.; Kinnarinen, T.; Häkkinen, A. Research Focus and Research Trends in Vacuum Filtration – Bibliographical Analysis. *Filtration* **2018**, *18*, 40–44.
[15] Sparks, T. Solid-Liquid Filtration: Understanding Filter Presses and Belt Filters. *Filtr. + Sep.* **2012**, *49* (4), 20–24. DOI: 10.1016/S0015-1882(12)70193-3.
[16] Sparks, T. (Trevor). *Solid-Liquid Filtration: A User's Guide to Minimizing Cost and Environmental Impact, Maximizing Quality and Productivity*; Butterworth-Heinemann: Oxford, 2012.
[17] Henriksson, B. Focus on Separation in the Mining Industry. *Filtr. Sep.* **2000**, *37* (7), 26–29. DOI: 10.1016/S0015-1882(00)80139-1.
[18] Besra, L.; Sengupta, D. K.; Roy, S. K. Particle Characteristics and Their Influence on Dewatering of Kaolin, Calcite and Quartz Suspensions. *Int. J. Miner. Process.* **2000**, *59* (2), 89–112. DOI: 10.1016/S0301-7516(99)00065-4.
[19] Kinnarinen, T.; Tuunila, R.; Häkkinen, A. Reduction of the Width of Particle Size Distribution to Improve Pressure Filtration Properties of Slurries. *Miner. Eng.* **2017**, *102*, 68–74. DOI: 10.1016/J.MINENG.2016.12.009.
[20] Tien, C. *Principles of Filtration*; Elsevier: Oxford, 2012.
[21] Wakeman, R. J.; Tarleton, E. S. Modelling, Simulation and Process Design of the Filter Cycle. *Filtr. Sep.* **1990**, *27* (6), 412–419. DOI: 10.1016/0015-1882(90)80534-R.
[22] Wakeman, R. J. An Improved Analysis for the Forced Gas Deliquoring of Filter Cakes and Porous Media. *J. Sep. Process Technol.* **1982**, *3* (1), 32–38.
[23] Hoşten, Ç.; Şan, O. Reassessment of Correlations for the Dewatering Characteristics of Filter Cakes. *Miner. Eng.* **2002**, *15* (5), 347–353. DOI: 10.1016/S0892-6875(02)00038-9.
[24] Wakeman, R. The Influence of Particle Properties on Filtration. *Sep. Purif. Technol.* **2007**, *58* (2), 234–241. DOI: 10.1016/J.SEPPUR.2007.03.018.
[25] Condie, D. J.; Hinkel, M.; Veal, C. J.; Boissy, K.; Leclerc, D. Modeling the Vacuum Filtration of Fine Coal. III. Comparison of Models for Predicting Desaturation Kinetics. *Sep. Sci. Technol.* **2000**, *35* (10), 1467–1484. DOI: 10.1081/SS-100100236.
[26] Fan, Y.; Dong, X.; Li, H. Dewatering Effect of Fine Coal Slurry and Filter Cake Structure Based on Particle Characteristics. *Vacuum* **2015**, *114*, 54–57. DOI: 10.1016/J.VACUUM.2015.01.003.
[27] Kemp, I. C. Reducing Dryer Energy Use by Process Integration and Pinch Analysis. *Dry. Technol.* **2005**, *23* (9–11), 2089–2104. DOI: 10.1080/07373930500210572.
[28] Kemp, I. C. Fundamentals of Energy Analysis of Dryers. In *Modern Drying Technology Volume 4: Energy Savings*; Wiley-VCH Verlag GmbH & Co. KGaA: Weinheim, Germany, 2012; pp 1–45. DOI: 10.1002/9783527631681.ch1.
[29] Svarovsky, L. *Solid-Liquid Separation*, 4th ed.; Butterworth-Heinemann, 2000.
[30] Tarleton, S.; Wakeman, R. *Solid/Liquid Separation : Principles of Industrial Filtration.*; Elsevier Science, 2005.

[31] Mujumdar, A. S. *Handbook of Industrial Drying*, 4rd ed.; CRC Press, 2014.
[32] Holdich, R. G. Solid–liquid Separation Equipment Selection and Modelling. *Miner. Eng.* **2003**, *16* (2), 75–83. DOI: 10.1016/S0892-6875(02)00178-4.
[33] Kudra, T.; Pallai, E.; Bartczaki, Z.; Peter, M. Drying of Paste-like Materials in Screw-Type Spouted-Bed and Spin-Flash Dryers. *Dry. Technol.* **1989**, *7* (3), 583–597. DOI: 10.1080/07373938908916612.
[34] Ryans, J. L.; Croll, S. Selecting Vacuum-Systems. *Chem. Eng.* **1981**, *88* (25), 72.
[35] Ryans, J.; Bays, J. Run Clean with Dry Vacuum Pumps. *CEP Magazine*. 2001.
[36] Taylor, J. L. An Operational Review of the Belt-Filtration Plant at Chemwes Limited. *J. South African Inst. Min. Metall.* **1983**, No. 10, 237–245.

This is an original manuscript of an article published by Taylor & Francis in Drying Technology on March 7, 2019, available online: http://www.tandfonline.com/doi/full/10.1080/07373937.2019.1581214.

Tables

Table 1. Actuator and sensor devices installed in the pilot-scale horizontal belt filter.

Device	**Manufacturer and model**	**Electrical motor**	**Variable speed drive**
Liquid ring vacuum pump	Robuschi RMV 14	Three-phase motor, 4.0 kW, 1430 rpm	ABB ACS580
Claw vacuum pump	Busch Mink MM1202AVA3	Three-phase motor, 5.1 kW, 3000 rpm	ABB ACS850
Slurry circulation pump	Larox LPP-D 20	Three-phase motor, 0.55 kW, 1400 rpm	Nordac SK300E
Slurry feed pump	Cole-Parmer Masterflex	Three-phase motor, 0.55 kW, 1360 rpm	ABB ACS580
Filter cloth drive	Heynau mini drive	Three-phase motor, 0.18 kW, 1400 rpm	ABB ACS580
Vacuum valves	Gemü		
Slurry control valves	Flowrox PVE25		
Bypass solenoid valve	Schmalz DRV 25 NC		
Cake thickness sensor	Keyence LB-1201 W		
Vacuum pump flow sensors	Schmidt SS 20.260		
Vacuum pressure difference transmitter	Aplisens APR-2000ALW		
Temperature sensors	Aplisens CT-I6		
Filtrate weight scale and transmitter	Dini Argeo PBE300 & DGT20AN		

This is an original manuscript of an article published by Taylor & Francis in Drying Technology on March 7, 2019,
available online: http://www.tandfonline.com/doi/full/10.1080/07373937.2019.1581214.

Table 2. Laboratory experiments carried out to study the material properties and energy consumption of cake dewatering using vacuum filtration. The equipment consisted of a Büchner apparatus and a pilot-scale horizontal belt vacuum filter.

Büchner experiments			**Pilot experiments, liquid ring pump**			**Pilot experiments, claw pump**		
Test	**Δp (bar)**	**w (kg/m^2)**	**Test**	**Δp (bar)**	**w (kg/m^2)**	**Test**	**Δp (bar)**	**w (kg/m^2)**
1	0.2	7.2	1	0.2	4.2	1	0.2	4.6
2	0.2	12.5	2	0.2	5.4	2	0.2	5.9
3	0.2	17.7	3	0.2	9.5	3	0.2	10.3
4	0.4	7.2	4	0.2	12.2	4	0.2	13.3
5	0.4	12.5	5	0.3	4.2	5	0.3	4.6
6	0.4	17.9	6	0.3	5.4	6	0.3	5.9
7	0.6	7.3	7	0.3	9.5	7	0.3	10.3
8	0.6	12.7	8	0.3	12.2	8	0.3	13.3
9	0.6	17.8	9	0.4	4.2	9	0.4	4.6
			10	0.4	5.4	10	0.4	5.9
			11	0.4	9.5	11	0.4	10.3
			12	0.4	12.2	12	0.4	13.3
						13	0.5	4.6
						14	0.5	13.3
						15	0.6	4.6
						16	0.6	13.3

Table 3. Büchner experiment variables, properties of the filter cakes, and separation time. Slurry temperature T = 22 °C and s = 25 wt.% in all experiments.

Test	**Δp (bar)**	**m_{sl} (g)**	**w (kg/m^2)**	**t_{sep} (s)**	**L_{meas} (mm)**	**$L_{tr,\,calc}$ (mm)**	**$\varepsilon_{av,\,meas}$ (-)**	**$\varepsilon_{av,\,tr,\,calc}$ (-)**	**$\alpha_{av} \cdot 10^{10}$ (m/kg)**
1	0.2	300	7.2	186	4.5	5.2	0.41	0.48	4.53
2	0.2	500	12.5	470	6.7	8.5	0.31	0.46	4.51
3	0.2	700	17.7	929	10.6	12.1	0.38	0.46	4.51
4	0.4	300	7.2	108	4.3	5.3	0.38	0.49	4.90
5	0.4	500	12.5	281	7.5	8.7	0.39	0.47	4.93
6	0.4	700	17.9	534	10.8	13.2	0.38	0.50	5.04
7	0.6	300	7.3	78	4.6	7.2	0.41	0.63	4.04
8	0.6	500	12.7	205	7.8	9.3	0.40	0.49	4.99
9	0.6	700	17.8	387	10.8	13.1	0.39	0.50	5.14

Table 4. Pilot experiments with a horizontal belt filter and a liquid ring vacuum pump. Slurry temperature T = 24 °C and s = 26 wt.% in all experiments.

Test	Δp (bar)	w (kg/m^2)	v_{belt} (cm/s)	t_f (s)	z_f (cm)	t_d (s)	z_d (cm)	L (mm)	ε_{av} (-)	M_s (g/s)	M (wt.%)
1	0.2	4.2	1.1	105	115	77	85	2.5	0.38	4.6	20.3
2	0.2	5.4	1.1	157	173	25	27	3.6	0.44	6.0	20.2
3	0.2	9.5	0.5	293	143	117	57	5.0	0.30	4.6	18.9
4	0.2	12.2	0.5	409	200	0	0	7.2	0.37	6.0	24.6
5	0.3	4.2	1.1	75	83	106	117	2.3	0.32	4.6	19.3
6	0.3	5.4	1.1	114	125	68	75	3.5	0.43	6.0	18.4
7	0.3	9.5	0.5	215	105	194	95	5.0	0.30	4.6	17.6
8	0.3	12.2	0.5	348	170	61	30	6.9	0.35	6.0	18.0
9	0.4	4.2	1.1	59	65	123	135	2.3	0.32	4.6	17.9
10	0.4	5.4	1.1	86	95	95	105	3.4	0.41	6.0	17.0
11	0.4	9.5	0.5	164	80	246	120	4.9	0.28	4.6	17.0
12	0.4	12.2	0.5	286	140	123	60	6.9	0.35	6.0	17.3

Table 5. Pilot experiments with a horizontal belt filter and a claw vacuum pump. Slurry temperature T = 22 °C and s = 28 wt.% in all experiments.

Test	Δp (bar)	w (kg/m^2)	v_{belt} (cm/s)	t_f (s)	z_f (cm)	t_d (s)	z_d (cm)	L (mm)	ε_{av} (-)	M_s (g/s)	M (wt.%)
1	0.2	4.6	1.1	105	115	77	85	3.3	0.48	5.0	19.4
2	0.2	5.9	1.1	164	180	18	20	4.2	0.48	6.5	19.5
3	0.2	10.3	0.5	276	135	133	65	6.3	0.39	5.0	17.9
4	0.2	13.3	0.5	409	200	0	0	8.1	0.39	6.5	22.7
5	0.3	4.6	1.1	77	85	105	115	3.2	0.47	5.0	18.1
6	0.3	5.9	1.1	118	130	64	70	4.0	0.45	6.5	17.8
7	0.3	10.3	0.5	225	110	184	90	6.1	0.37	5.0	16.9
8	0.3	13.3	0.5	358	175	61	25	7.7	0.36	6.5	17.6
9	0.4	4.6	1.1	59	65	123	135	3.1	0.45	5.0	17.0
10	0.4	5.9	1.1	100	110	77	90	3.9	0.44	6.5	16.7
11	0.4	10.3	0.5	184	90	225	110	5.8	0.34	5.0	16.4
12	0.4	13.3	0.5	286	140	123	60	7.6	0.35	6.5	16.6
13	0.5	4.6	1.1	55	60	127	140	2.9	0.41	5.0	16.4
14	0.5	13.3	0.5	235	115	174	85	7.3	0.33	6.5	16.3
15	0.6	4.6	1.1	50	55	132	145	2.8	0.39	5.0	15.4
16	0.6	13.3	0.5	215	105	194	95	7.2	0.32	6.5	16.0

Table 6. Measured standard volumetric air flow rates for the total flow through the vacuum pump, the estimated volumetric air flow rate, and the air flux through the filter cake dewatering area calculated on the basis of leak flow measurements.

Liquid ring vacuum pump experiments						**Claw vacuum pump experiments**					
Test	**Δp (bar)**	**w (kg/m^2)**	**$Q_{a,\,total}$ (m^3/h)**	**$Q_{a,\,cake}$ (m^3/h)**	**$u_{a,\,cake}$ (m^3/h·m^2)**	**Test**	**Δp (bar)**	**w (kg/m^2)**	**$Q_{a,\,total}$ (m^3/h)**	**$Q_{a,\,cake}$ (m^3/h)**	**$u_{a,\,cake}$ (m^3/h·m^2)**
1	0.2	4.2	35.0	2.0	23.7	1	0.2	4.6	31.5	3.5	41.3
2	0.2	5.4	33.5	0.5	19.0	2	0.2	5.9	29.2	1.2	60.6
3	0.2	9.5	36.0	3.0	52.8	3	0.2	10.3	33.7	5.7	87.9
4	0.2	12.2	33.0	0.0	-	4	0.2	13.3	28.0	0.0	-
5	0.3	4.2	45.0	4.9	42.1	5	0.3	4.6	41.0	5.9	51.5
6	0.3	5.4	43.0	2.9	39.0	6	0.3	5.9	40.0	4.9	70.3
7	0.3	9.5	49.0	8.9	93.9	7	0.3	10.3	45.5	10.4	115.8
8	0.3	12.2	43.5	3.4	114.1	8	0.3	13.3	38.8	3.7	124.1
9	0.4	4.2	53.0	5.8	43.2	9	0.4	4.6	49.0	6.8	50.6
10	0.4	5.4	55.0	7.8	74.6	10	0.4	5.9	48.5	6.3	74.5
11	0.4	9.5	63.0	15.8	132.0	11	0.4	10.3	55.5	13.3	121.2
12	0.4	12.2	57.0	9.8	163.9	12	0.4	13.3	50.0	7.8	130.6
						13	0.5	4.6	56.0	6.7	48.2
						14	0.5	13.3	58.0	8.7	102.9
						15	0.6	4.6	66.0	9.7	66.6
						16	0.6	13.3	65.0	8.7	91.1